Deuterium uptake during Pd–D codeposition

S. Szpak [a], P.A. Mosier-Boss [a], J.J. Smith [b]

[a] Naval Command, Control and Ocean Surveillence Center, RDT&E Division, San Diego, CA 92152-5000, USA
[b] Department of Energy, Washington, DC 20585, USA

ABSTRACT

The mode of deuterium uptake during Pd–D co–deposition has been explored using galvanostatic perturbation techniques. The resultant potential relaxation curves exhibit four distinct potential—time intervals where the relaxation process is controlled by the interaction between the transport of deuterium from the lattice to the surface to form adsorbed deuterium and the reduction of palladium from solution. These interactions are discussed in terms of the palladium + electrolyte interphase.

1. INTRODUCTION

Although the hydrogen evolution reaction has been studied extensively since the turn of the century, details of how to maintain, for example, a high surface coverage of adsorbed hydrogen and, in the case of the Pd electrode, to promote a high ratio of absorbed hydrogen to palladium remain unclear. Recently, we described sorption of electrochemically generated deuterium in terms of interfacial events [1] and emphasized the role of the interphase [2]. Of particular interest is the significantly higher efficiency of electrochemical charging compared with that of charging from the gas phase [3]. This poses the question as to what role, if any, the electrode potential plays in maintaining a high D/Pd atomic ratio. It is often assumed that there is little difference, apart from the usual isotopic effect, between the behavior of the Pd + H system, where a great deal of information is available, and that of the Pd + D system. However, this assumption, is not always valid; for example, Rolison et al. [4] clearly illustrated the difference in the development of surface morphology associated with a prolonged evolution of deuterium and hydrogen on Pd cathodes.

In this paper, we explore the mode of deuterium uptake during the process of Pd–D codeposition. The sequence of events is expected to be the same as in the charging of a solid electrode but they should be more clearly defined because of the formation of a new electrode surface which is not affected by prolonged contact with solution.

2. EXPERIMENTAL AND RESULTS

The experimental approach selected here is that of the examination of the electrode response to a programmed constant current pulse. The corresponding time rate of change of the electrode potential, measured versus a reference electrode, provides the required information on the participating processes.

2.1. Cell, Apparatus, Pulse Generation and Recording

A two–compartment glass cell, separated by a fritted disk, was used. The working electrode consisted of a set of 14 Pt wires, 0.05 cm in diameter ($A = 1.96 \times 10^{-3}$ cm^2), embedded in an acrylic block and separately connected through a switching arrangement to a controlled power source. The Pt wire electrodes were separated from each other by a distance of 3 mm and were arranged in two rows 8.5 mm apart. The counter–electrode and reference electrode were respectively a Pt mesh and Ag | AgCl in saturated KCl dissolved in D_2O. An unstirred D_2O solution, 0.05 M in $PdCl_2$ and 0.3 M in LiCl, served as the electrolyte. Current pulses were generated by a computer–driven potentiostat (PAR model 173) with a 276 IEEE computer interface.

2.2. Charging Curves and Potential Relaxation

A summary of the electrode potential response $\Phi(t)$ to the perturbation in the form of a constant current density pulse j and the return to equilibrium condition is shown in Fig. 1. Typically, on charging, four distinct time intervals can be identified in which the $\Phi(t)$ function differs. The first time interval, $0 < t < t_1$, is characterized by a rapid change in Φ and exhibits an extremum at Φ_1, point A. This is followed by an interval tl $t_1 < t < t_2$, where the electrode potential asymptotically approaches a constant value Φ_2. In the remaining two time intervals, $t_2 < t < t_3$ and $t_3 < t < t_4$, the $\Phi(t)$ relation is almost linear but with slightly different slopes. The interphase relaxation behavior, displayed in the form of $\Phi(t)|_{j=0}$ and $\Phi(t)|_{j>0}$, is shown in Fig. 1 by the broken curves a, b, c, and a$'$, b$'$, c$'$ respectively. The complexity of the relaxation process increases with the current pulse duration. When the current flow is interrupted before the first plateau is reached, i.e. along the asymptotic approach, the potential relaxes in a manner resembling an exponential relation (curve a).
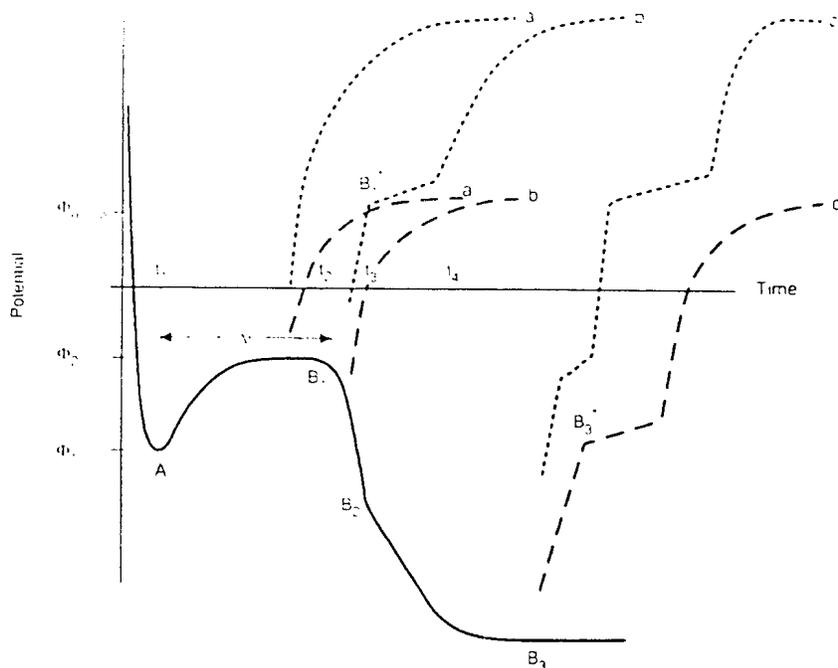
Figure 1. Idealized representation of the $\Phi(t)$ response to a galvanostatic pulse (solid curve) and the $\Delta\Phi(t)$ relaxation on current interruption at points indicated (broken curves): point A, onset of crystallization (nucleation); period Δt represents an asymptotic approach to a complete coverage by PdD_x deposit; points $B_1, B_2, ..., B_1^*$ indicate a change in the reaction path. Curves a, b, c for $\Phi(t)|_{j=0}$; curves a$'$, b$'$, c$'$ for $\Phi(t)|_{j>0}$.

Qualitatively, the shape of the $\Phi(t)$ curve is independent of the magnitude of the applied cathodic current density pulse; the duration of the characteristic time intervals decreases almost exponentially with increases in pulse current. For example, the onset of crystallization (Fig. 1, point A) occurs at 230 ms when the current density pulse j is -5×10^{-3} A cm^{-2} and shortens to 1.2 ms when $j = -2 \times 10^{-1}$ A cm^{-2}. This behavior indicates that an increase in the magnitude of current density pulse leads to a compression in time which, if not accounted for, can result in a loss in resolution of the relaxation curves. Also, as in the case of charging, the potential relaxation is characterized by well–defined regions. These regions are associated with a change in the reaction path as the electrode returns to its rest potential or is forced to a new stationary state.

3. FACTORS AFFECTING THE SHAPE OF THE CHARGE–DECAY CURVES

In interpreting the $\Phi(t)$ curves in terms of the dynamics of the interphase region, we first review factors pertinent to the D–Pd codeposition process, namely reaction paths, kinetics of deuterium evolution with emphasis on the associated surface coverage, and the structure of the interphase and its simulation by an electric circuit analog.

3.1. Reaction Paths

Reactions participating in the Pd–D codeposition are the reduction of Pd^{2+} ions

$$Pd^{2+} + 2e^- \rightarrow Pd^0 \quad j_{0,1}, \eta_1 \quad \eta_i = \Phi_i - \Phi_{rev,i} \tag{I}$$
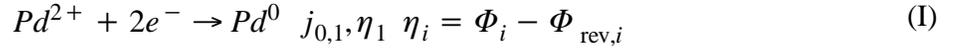
and the reduction of heavy water

$$D_2O + e^- \rightarrow D(a) + OD^- \quad j_{0,2}, \alpha_2, \eta_2 \tag{II}$$

$$D_2O + D(a) + D(a) + e^- \rightarrow D_2(s) + OD^- \quad j_{0,3}, \alpha_3, \eta_2 \tag{III}$$
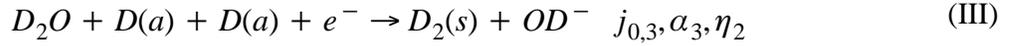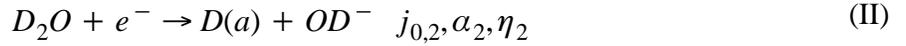
followed by the evolution and absorption of deuterium

$$D(a) + D(a) \rightarrow D_2(s) \quad j_{0,4}, (k_4, k_{-4}) \tag{IV}$$

$$D(a) \rightarrow D(l) \quad j_{0,5}.(k_5, k_{-5}) \tag{V}$$
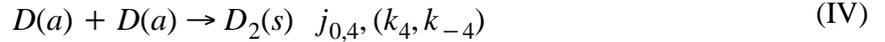
where (a), (s) and (l) denote adsorbed, solution and lattice species. The charge transfer processes (Eqs. (I)—(III)) occur independently, i.e. the overall charge transfer process is viewed as the sum of the respective individual contributions.

3.2. Electrode Kinetics: Basic Equations

When considering the Pd deposition in the presence of evolving deuterium, it is sufficient to take into account those events that follow the formation of Pd adions/adatoms. If similar with other electrocrystallization processes, the rate–controlling path for the reduction of Pd^{2+} ions may proceed via surface diffusion or by charge transfer control [5]. Under normal circumstances, surface diffusion is the controlling factor. During codeposition, and within the current density pulse duration where the evolution of surface morphology dominates, charge transfer control is favored:

$$j_1 = -j_{0,1} \exp\left[-(1-\alpha_1)\right] f \eta_1 \tag{1}$$

where $f = F/RT$.

The surface activities of freshly deposited Pd are coupled with individual processes associated with deuterium evolution, namely charge transfer at points where no D is present (Eq. (II)) or at points where D is present (Eq. (III)) , recombination (Eq. (IV)), or desorption of D_2 by diffusion into the liquid phase or removal by bubble formation. During codeposition, two cases can be distinguished: deuterium evolves (i) on a totally bare electrode surface (Volmer path)

$$j_2 = -j_{0,2}(1 - \theta) \exp\left[-(1 - \alpha_2)\right] f\eta_2 = (1 - \theta)j_2(\eta_2) \tag{2}$$

or (ii) on occupied sites (Heyrovsky path)

$$j_3 = -j_{0,3}\theta \exp\left[(-(1 - \alpha_3)\right] f\eta_3 = \theta j_3(\eta_3) \quad \eta_2 \approx \eta_3 \tag{3}$$

yielding the total current of deuterium evolution

$$j_2 + j_3 = j_2(\eta_2) + \theta[j_3(\eta_2) - j_2(\eta_2)] \tag{4}$$

The precise form of the $j(\eta)$ relationship is less important than the relative ratio of the partial currents, $j_1/(j_2 + j_3)$. However, while examining the dynamics of the interphase during codeposition, attention should be directed to ascertaining how the density of D adsorption active sites relates to the overpotential and the rate of Pd deposition. Because of the continuous formation of a new surface, the electrode area grows, thereby reducing the overpotential as well as the exchange current density with respect to that existing immediately before. Small changes in surface area may produce substantial changes in local $j_{0,1}$ which, in turn, will give rise to a non–uniform distribution of charge transfer current density. Also, the activity of the surface is strongly affected by the growth form and, through it, by the density of surface defects.

3.3. Structure of the Interphase

Thermodynamic considerations relate the measured potential to the affinity of the elementary charge transfer processes [6,7]. Consequently, the structure and properties of the Pd + H_2O interphase can be derived from analysis of a charged Pd electrode responding to anodic currents. On this basis, Bucur and Bota [8] concluded that there is an accumulation of hydrogen on the metal side of the interphase and that the mobility of the adsorbed hydrogen affects the transfer equilibria. They also noted the effect of surface morphology; in particular, they suggested that the surface of black Pd acts as a hydrogen trap when in contact with an electrolyte but not when in contact with a gaseous phase. Somewhat later, Schlapbach [9] presented the following picture. The equilibrium position of the hydrogen surface atoms is different from that given by lattice periodicity in the bulk. Further, with an increase in the surface coverage, adsorbed H atoms form both disordered and ordered phases. He also noted that adsorption can induce relaxation (or reconstruction) of the surface, i.e. it can be viewed as adsorption–absorption induced alteration of structure (change in the inhomogeneity of material). Chemisorbed hydrogen occupies sites on top of the first layer and also sites between and underneath the top surface atoms, i.e. in agreement with hydrogen accumulation on the metal side [8].

As previously [2,10], we stress the nonautonomous character of the Pd + D interphase and note its active participation during transport of interstitials. The nonhomogeneity of the deuterium distribution may extend further into the bulk because spatial structures can be generated due to a concentration–dependent diffusion coefficient, thus contributing to the complex behavior of the interphase [11]. As a rule, investigation of the behavior and properties of the electrode + electrolyte interphase is limited to examination of the solution side [7]. The reason for this approach is that the electric field does not affect thermodynamic properties of metals. However, for hydrogen absorbing electrodes, a case can

be made that the external electric field penetrates the interphase to some extent, especially during the transport across the interphase. The ensuing concentration gradients make the electrode inhomogeneous with respect to its composition. Furthermore, the driving force is the gradient of the chemical potential in the bulk only if the electric field does not affect the energetics of the system, i.e. if the action of the electric field does not polarize molecules. The question that arises is whether or not the molecules/atoms within the interphase are polarized; if they are, then the strength of the electric field must be included when discussing the uptake of deuterium. Consequently, the relative importance of mechanical distortion of the lattice and of the electric field must be assessed.

3.4. ELECTRIC CIRCUIT ANALOG

When the adsorbed species participate in the charge transfer process, the electrode surface itself can be regarded as either a reactant or a product. Thus its properties enter into the formulation of the appropriate rate equations. In the case of adsorbed reactants, the overall reaction path and the sequence of events are derived from the basic relation $\Phi(t) = \Phi(\theta_1, \theta_2 ..; j_1, j_2,...)$. A somewhat simpler functional dependence can be formulated for Pd–D codeposition. Although there are five reaction paths, and therefore five fluxes, there is only one surface coverage θ of interest, that of adsorbed deuterium. A common time–dependent Galvani potential difference $\Phi(t)$ drives three reactions, represented by Eqs. (I)—(III), through two overpotentials η_1, η_2. Thus we can write

$$\Phi(t) = \Phi[\theta; j_1(\eta_1), j_2(\eta_2), j_3(\eta_2)] \tag{5}$$

Following the differentiation of Eq. (5)

$$\frac{d\Phi}{dt} = \frac{\partial\Phi}{\partial\theta}\Big|_{j_1,j_2...}\frac{d\theta}{dt} + \sum_i \frac{\partial\Phi}{\partial j_i}\Big|_{theta, j\neq j_1}\frac{dj_1}{dt} \quad i = 1, 2, 3 \tag{6}$$

we assign a physical meaning to each term on the right–hand side and interpret the $\Phi(t)$ behavior via the use of an electric circuit analog. To derive this analogy, we employ, as in our previous paper [1] the conservation of charge

$$C\frac{d\Phi}{dt} = j - (j_1 + j_2 + j_3) \tag{7}$$

and the deuterium mass balance

$$\Gamma_m F\frac{d\theta}{dt} = j - (j_1 + j_2 + j_3) \tag{8}$$

Combining Eqs. (7) and (8), we eliminate one partial current (either j_2 or j_3) and obtain

$$C\frac{d\Phi}{dt} \pm \Gamma_m F\frac{d\theta}{dt} = j^* \tag{9}$$

where C is the effective potential–independent capacitance on the solution side of the interphase, Γ_m is the maximum number of sites per unit area and j* is the sum of rates of all but one of the processes expressed as currents and the plus or minus sign indicates the way in which Eqs. (7) and (8) were combined (i.e. by addition or subtraction). Solving for $d\theta/dt$ and substituting in Eq. (6), we obtain

$$\left(1 \pm \frac{C\partial\Phi}{\Gamma_m F\partial\theta}\right)\frac{d\Phi}{dt}$$

$$= \frac{j^*}{\Gamma_m F}\frac{\partial\Phi}{\partial\theta}\Big|_{j_1,...} + \sum_{j\neq j_i}\frac{\partial\Phi}{\partial j_i}\Big|_{\theta, j_1, j_2,...}\frac{dj_i}{dt} \tag{10}$$

Identifying the term $(1/\Gamma_m F)(\partial\Phi/\partial\theta)$ with the adsorption capacitance C_{ad}^{-1} and taking $C_{ad} \gg C$ and $\partial\Phi/\partial_{ji} = R_i$, we further simplify to obtain

$$\frac{d\Phi}{dt} = \frac{j*}{C_{ad}} + \sum R_i \frac{dj_i}{dt} \qquad (11)$$

where the R_1 are the respective faradaic resistances.

4. INTERPRETATION OF THE Φ(T) CURVES

The events associated with the deuterium uptake in the course of Pd–D codeposition are derived from the characteristic features of $\Phi(t)$ curves. Three features are examined: the change in slope, the amount of absorbed deuterium, determined by anodic pulse current, and the transport of deuterium within the interphase.

4.1. Change in Slope

A common feature observed in all cases of charging and discharging, to a varying degree, is the change in the slope of the $\Phi(t)$ curve which, in turn, is related to the change in the reaction path (Eq. (11)). To simplify the mathematics, we consider the potential relaxation under zero external cell current, ($j = 0$). Under this condition, $\Phi(t)$ is viewed as a mixed potential which, in the absence of Pd^{2+} ions, arises from two partial currents: oxidation of deuterium via the Volmer path and reduction via the Heyrovsky path [12]. In the presence of Pd^{2+} ions, the cathodic partial current $-j_1$ replaces the Heyrovsky path and drives the oxidation of deuterium with the current j_2; the deuterium is supplied to the charge transfer plane by transport from the metal side of the interphase $j*$. Accordingly, Eq. (11) becomes

$$\frac{d\Phi}{dt} = \frac{j*}{C_{ad}} + \left(\frac{\partial\Phi}{\partial j_i}\frac{dj_1}{dt} + \frac{\partial\Phi}{\partial j_2}\frac{dj_2}{dt} \right) \qquad (12)$$

which, with $j_1 + j_2 = 0$, yields $dj_1/dt = -dj_2/dt$, resulting in

$$\frac{d\Phi}{dt} = \frac{j*}{C_{ad}} + (R_1 - R_2)\frac{dj}{dt} \qquad (13)$$

Eq. (13) implies that the observed change in the slope of the $\Phi(t)$ curves, on either charge or discharge, must be attributed to a change in the reaction path. This conclusion is supported by the fact that at the point of change (e.g. points B_1 and B_2 in Fig. 1) conditions at the charge transfer surface remain unchanged; consequently, the term $j*/C_{ad}$ in Eq. (13) could not be substantially affected.

4.2. Deuterium Uptake

Scanning electron microscope examination of the surface revealed that, within the first time interval, as the $d\Phi(t)/dt$ asymptotically approaches zero, the Pd deposition (and/or PdD_x codeposition) proceeds via nucleation with overlapping layers. During this period, the $\Phi(t)$ curve is dominated by the surface coverage which obeys Eq. (8) and which, after neglecting contributions due to the Heyrovsky and Tafel paths, yields

$$\Gamma_m F \frac{d\theta}{dt} = j_2(1 - \theta) - k_5\theta - j_1\theta \qquad (14)$$

where the first term on the right–hand side denotes an increase in surface coverage arising from the Volmer path, the second term reduces it by absorption and the third term reduces it further by creating

new surface (i.e. new adsorption sites). Viewing the codeposition as one–dimensional growth, the term θ is, in fact, the fraction of sites occupied by the absorbed deuterons (ξ in Ref. 1). If we take its value as zero at point A in Fig. 2, an integration of Eq. (14) yields

$$\theta(t) = \frac{j_2}{j_2 + k_5 + j_1}\left[1 - \exp\left(-\frac{j_2 + k_5 + j_1}{\Gamma_m F}t\right)\right]$$

(15)

Eq. (15) implies that a change in composition of the codeposited PdD_x should follow the change in the $\Phi(t)$ curve, i.e. should approach saturation asymptotically. The D/Pd atomic ratio along the asymptote can be determined by reversing the current flow. The results of such current reversal are illustrated in Fig. 2 where a charging current of 5×10^{-3} A cm^{-2} was selected to display the progression of deuterium loading and the reversal was made at the points indicated. The D/Pd, ratios, where $D = D(a) + D(l)$, calculated from the Q_a/Q_c ratio were 0.42, 0.68, 0.98 and 1.02 at the times indicated. Further, Eq. (15) is in agreement with the observed effect of the pulse current density $-j_1$ on the initial behavior of the $\Phi(t)$ curve.
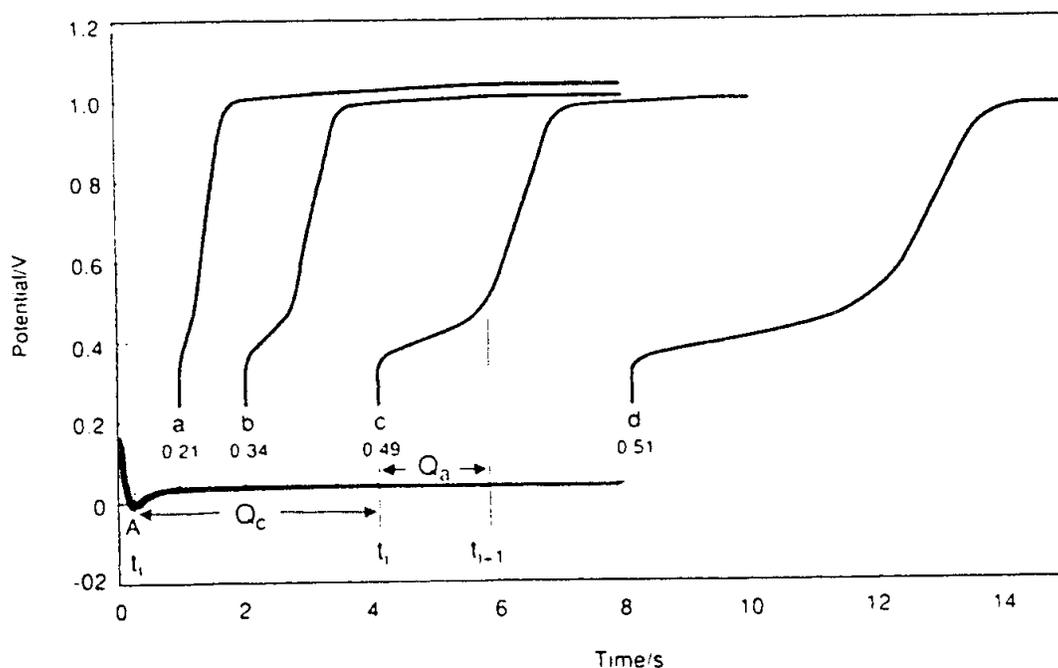
Figure 2. The $\Phi(t)$ behavior upon cell current reversal following various times of codeposition process. Determination of D/Pd atomic ratio. Cathodic current density $j = -5 \times 10^{-3}$ A cm^{-2}; anodic current density $j = 5 \times 10^{-3}$ A cm^{-2}; cell current reversal at 1, 2, 4 and 8 s; corresponding $\Phi(t)$, curves a, b, c and d respectively. Ratio $Q_a/Q_c = j(t_{i+1} - t_i)/|-j(t_i - t_1)|$ is indicated.

It can be seen that Eq. (15) represents the situation well at the beginning of the codeposition. Immediately after the onset of crystallization there is an increase in the electrode area with concurrent lowering of the overpotential and a rapid adsorption of deuterium. This rapid adsorption of deuterium early in the process is also supported by cyclic voltammetry [13] and X–ray diffraction [14] data. The fall in overpotential is attributed to both the expansion of the surface area and the adsorption of deuterium. The effect of $-j_1$ is via the generation of new surface sites affecting reactions (II) and (III) but the functional relation is not clear at this time. As a first approximation, we assume the simplest relation between the rate of Pd deposition and the formation of new adsorption sites, that of

proportionality, i.e. $(1 - \theta)$ α–j_1 which, in turn, accelerates the Volmer reaction and slows down remaining paths.

4.3. Deuterium Transport Within the Interphase

Limited information on deuterium transport within the Pd lattice and across the interphase can be derived by examining the electrode response after current reversal. The uniform composition of the PdD_x is consistent with the rapid sorption of deuterium into the freshly deposited Pd. At the moment of the cathodic current interruption, the amount of sorbed deuterium, expressed in terms of the charge transferred, is $Q_D = -(j_2 + j_3)/t$. Following the cell current interruption, the $\Phi(t)$ curves can be examined under conditions of either zero cell current (Fig. 3) or cell current reversal (Fig. 4).

In the first case, each $\Phi(t)$ curve exhibits two features: (i) approximately linear regions, AB and BC, with changing slope at point B, and (ii) decreasing slopes of these segments, as shown in Table 1, with increasing length of the codeposition period, i.e. with the thickness of the PdD_x layer. By Eq. (13), with $j = 0$, the linear segments of the $\Phi(t)$ curves imply that the change in partial current(s) is compensated by the j^* term since C_{ad} remains essentially constant. This compensation occurs via the generation of surface active sites and the resupply of deuterium to the charge transfer plane. The linear relation can be maintained only if the supply of deuterium from the interior to the charge transfer plane is fast, i.e. if $j^* \gg |-j_1|$. The second characteristic point, i.e. the decrease in slope with an increase in the codeposition time, is also consistent with uniform distribution of absorbed deuterium through the growing PdD_x layer and the fast equilibration between the lattice deuterium D(l) and the adsorbed deuterium D(a). It is noteworthy that the approach to the rest potential does not follow the square–root dependence or the logarithmic relationship, thus indicating coupling between bulk and surface processes at all times. During this time, as the potential approaches constant value, the rate at which D(a) reacts further, i.e. the equilibration between sorbed and adsorbed deuterium is faster than subsequent D(a) reactions.

The effects of an anodic current following the termination of the codeposition on the $\Phi(t)$ curves are shown in Fig. 4. In particular, the electrode responses to $j = 5.0 \times 10^{-3}$ A cm^{-2} and $j = 10^{-2}$ A cm^{-2} are compared with the response to zero cell current. Several features are noteworthy. First, the general shape of the relaxation curve is unchanged. However, the slopes of the segments are steeper owing to forced oxidation of adsorbed deuterium D(a), and the amount of recovered (oxidized) deuterium is less which indicates that the supply of deuterium from the bulk to the metal side of the interphase is replaced by diffusion. The latter does not invalidate the fast exchange between the D atoms within the interphase and those populating the charge transfer surface sites.

The anodic $\Phi(t)$ curves provide a qualitative measure of the respective processes. Of interest is the appearance of a third segment, which is particularly pronounced at $j = 10^{-2}$ A cm^{-2} (Fig. 4). Since there are only two distinct paths associated with either reduction or oxidation, this new feature represents either the order–disorder phase transition [9] or the existence of energetically different states of the adsorbed deuterium [13].

5. CONCLUDING REMARKS

Models for the $PdD_x + D_2O$ interphase suggest fine spatial structure (as far as D concentration is concerned), i.e. the interphase consists of laminae which are homogeneous with respect to deuterium concentration. The interphase is characterized as follows.

(1)   The nonautonomous character of the interphase and its active participation in the course of sorption is accentuated by the codeposition process.
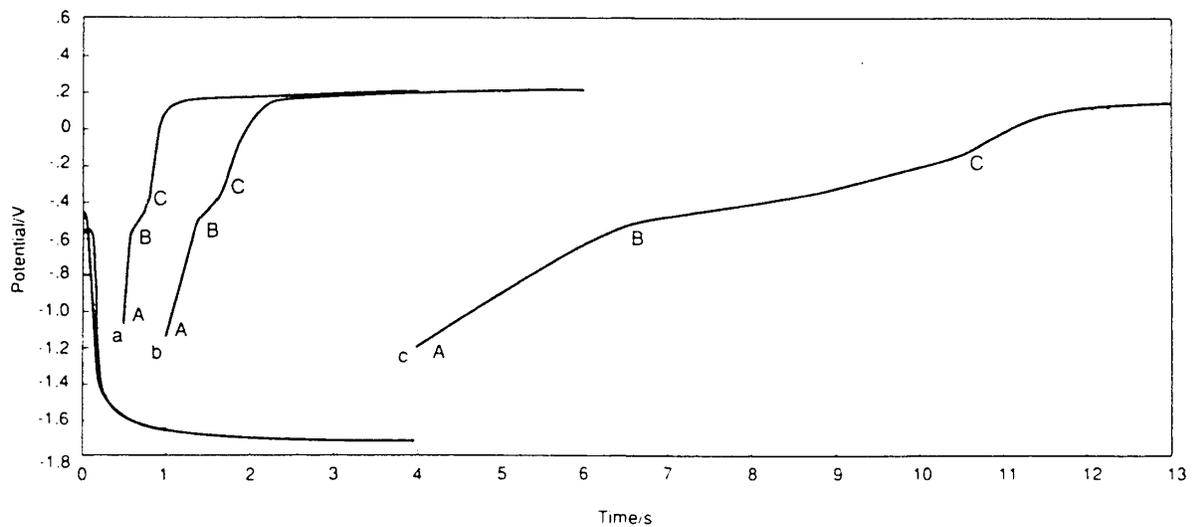
Figure 3. Approach to electrode rest potential $\Phi(t)|_{j=0}$ upon termination of the codeposition. Cathodic current density $j = -10^{-1}$ A cm^{-2} terminated at 0.5 s, 1 s and 4 s (curves a, b, and c respectively).
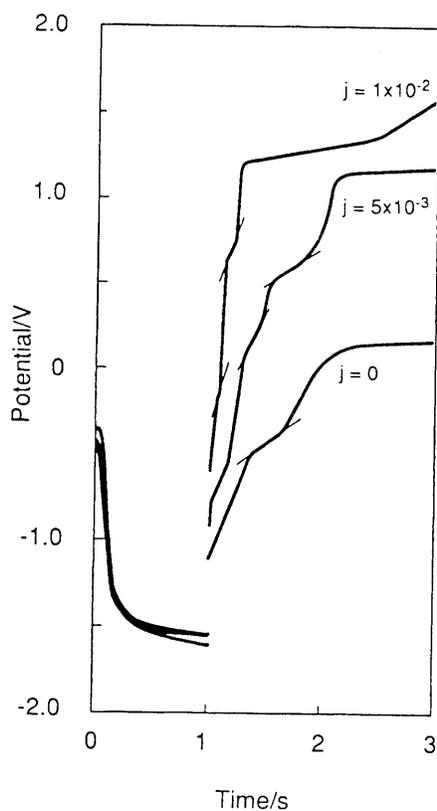
Figure 4. The $\Phi(t)$ behavior as a function of current reversal (indicated): codeposition current density $j = -10^{-1}$ A cm^{-2}; codeposition time, 1 s.

Table 1. Slopes of linear segments, AB + BC in Fig. 3, as a function of Q.

$Q(/As)$	Segment AB (V/s^{-1})	Segment BC (V/s^{-1})
2×10^{-5}	23.0	7.30
4×10^{-5}	11.1	3.17
10^{-4}	5.6	0.7
2×10^{-4}	1.8	0.53
8×10^{-4}	0.27	0.08

(2)   The surface–controlled sorption rates (e.g. metal–hydrogen energy conversion systems) are of technological importance.

(3)   The $\Phi(t)$ curves display changes in the reaction paths as well as the complexity of the inter-phase region.

ACKNOWLEDGEMENT

REFERENCES

1.   S. Szpak, C.J. Gabriel, J.J. Smith and R.J. Nowak, J. Elec— troanal. Chem., 309 (1991) 273.

2.   S. Szpak, P.A. Mosier—Boss, S.R. Scharber and J.J. Smith, J. Electroanal. Chem., 337 (1992) 273.

3.   M. Smialowski, Hydrogen in Steels. Pergamon. London, 1962. Ch.3.

4.   D.R. Rolison, W.E. O'Grady. R.J. Doyle and P.P. Trzaskoma, Proc. 1st Conf. on Cold Fusion, Salt Lake City. UT. National Cold Fusion Institute. 1990.

5.   J.O'M. Bockris and G.A. Razunaney. Fundamental Aspects of Electrocrystallization, Plenum Press, New York, 1967.

6.   M. Enyo and T. Maoka, J. Electroanal. Chem.. 108 (l980) 277. [7] P. van Rysselberghe in J.O'M. Bockris (Ed.), Modern Aspects of

7.   Electrochemistry, Vol. 4, Plenum, New York. 1966.

8.   R.V. Bucur and F. Bota, Electrochim. Acta. 28 (1983) 1373; 29 (1984)103.

9.   L. Schlapbach in T. Bressani, E. Del Giudici and G. Preparala (Eds.) in The Science of Cold Fusion, SIF. Bologna, 1991

10. S. Szpak. P.A. Mosier—Boss, S.R. Scharber and J.J. Smith, J. Electroanal. Chem., in press.

11. A.L. Samgin, V.I, Tsidlikovski and A.N. Baraboshkin, Proc. 3rd Int. Conference on Cold Fusion, Nagoya, Japan, Universal Academy Press, Inc., Tokyo. 1993.

12. K.J. Vetter, Electrochemical Kinetics, Academic Press, New York. 1967, p. 607.

13. S. Szpak, P.A. Mosier—Boss, S.R. Scharber and J.J. Smith, J. Electroanal. Chem., in press.

14. S. Szpak, P.A. Mosier—Boss and J.J. Smith. J. Electroanal. Chem., in press.